ASTRONOMY & ASTROPHYSICS
SUPPLEMENT SERIES

Astron. Astrophys. Suppl. Ser. **125,** 293-301 (1997)

Near infrared H and K' surface photometry of three Tully-Fisher calibrators: NGC 2366, NGC 2403 and NGC 4236⋆

D. Pierini[1,2], **G. Gavazzi**[1,2], **A. Boselli**[3,4,5], **and R. Tuffs**[3]

[1] Università degli Studi di Milano, Via Celoria 16, 20133, Milano, Italy
[2] Osservatorio Astronomico di Brera, Via Brera 28, 20121 Milano, Italy
[3] MPI für Kernphysik, Postfach 103980, D–69117 Heidelberg, Germany
[4] DEMIRM, Observatoire de Paris, 61 Av. de l'Observatoire, 75014 Paris, France
[5] present address: Laboratoire d'Astronomie Spatiale, Traverse du Siphon, F-13376 Marseille Cedex 12, France

Received November 6, 1995; accepted November 26, 1996

Abstract. Near Infrared H and K' surface photometry of the three nearby galaxies NGC 2366, NGC 2403 and NGC 4236, used as local calibrators of the Tully-Fisher relation, was obtained using the 256^2 NICMOS3 IR array MAGIC attached to the 2.2 m telescope of Calar Alto. The present measurements are compared with the aperture photometry available in the literature. Surface brightness profiles and integrated magnitudes are given.[1]

Key words: galaxies: photometry — galaxies: NGC 2366, NGC 2403, NGC 4236 — infrared: galaxies

1. Introduction

The empirical correlation between the luminosity of spiral galaxies and their rotational velocity, named as "Tully-Fisher" relation (TFR) (Tully & Fisher 1977), provides us with a method for estimating distances of galaxies on scales of cosmological interest. While its slope can be determined with high statistical significance using galaxies in several "well-behaved" (without substructure) clusters, distributed with a large distance spread ($0-10000$ km s^{-1}) (Aaronson et al. 1986; Gavazzi et al. 1991), the determination of the zero-point relies on measurements of few nearby galaxies whose distances are accurately known by means of primary distance indicators.

In particular the parameters of the infrared H band ($1.65\,\mu$m) TFR were derived by Aaronson et al. (1980) (hereafter AA80) using aperture photometry measurements of 12 nearby galaxies, several of which had the distance determined with the Cepheids method. A consistent calibration was obtained by Freedman 1990 who used 4 galaxies in common with AA80 (M 31, M 33, NGC 2403, M 81) adopting distance moduli redetermined with new data for Cepheids and the H aperture photometry of AA80.

Given the direct impact of the TFR zero-point on the determination of H_0, it is crucial to try to improve the IR photometry of the TF calibrators using the panoramic infrared detectors which recently became available in large format (256^2). This method offers some obvious advantages over aperture photometry, allowing i) the determination of $H_{-0.5}$ with no growth-curve extrapolation and ii) accurate subtraction of unwanted contaminating stars in the field (see also Peletier & Willner 1993).

In this paper we present the first surface brightness near-infrared measurement of three TF calibrators in the NGC 2403-M 81 group: NGC 2403 itself, NGC 2366 and NGC 4236. H band measurements are checked against the aperture photometry of AA80. Meanwhile, given the growing importance in extragalactic studies of the new K' band filter ($2.1\,\mu$m) (Wainscoat & Cowie 1992), which was designed to suppress part of the thermal background dominating the IR ground-based observations, we also obtained frames of the three galaxies with this filter.
We were able to photograph the large galaxies of this study, some of which span almost 20 arcmin in the sky, as a side-product of a project aimed at observing late-type Virgo Cluster galaxies (Boselli et al. 1997).

Send offprint requests to: D. Pierini

⋆ based on observations taken at the Calar Alto Observatory, operated by the Max Planck Institut für Astronomie (Heidelberg) jointly with the Spanish National Commission for Astronomy.

[1] The tables are also available at the CDS via anonymous ftp to cdsarc.u-strasbg.fr (130.79.128.5) or via http://cdsweb.u-strasbg.fr/Abstract.html

2. Observations and image reduction

Observations of the three galaxies reported in this paper were carried out in the photometric night of Feb. 25, 1994, with the Calar Alto 2.2 m telescope equipped with the MAGIC NICMOS3, 256^2 pixels infrared array (Herbst et al. 1993). The optical set-up of the detector was chosen to give the largest possible field of view (6.8×6.8 arcmin^2), with a pixel size of 1.61 arcsec. The expected deviation from linearity of the detector is $\sim$0.5% at the count rate of the present observations.
Table 1 lists the relevant parameters of the galaxies observed in this work. The table is arranged as follows:
Column 1: NGC denominations;
Columns 2, 3: adopted (1950) celestial coordinates;
Columns 4, 5: major and minor diameters as given in the RC2 (de Vaucouleurs et al. 1976);
Column 6: morphological type.

Table 1. Galaxy parameters

	Celestial coordinates (1950)				
NGC	R.A. h m s	DEC ° ′ ″	a_{25} arcmin	b_{25} arcmin	type
2366	07 23 38.00	69 19 15.0	7.59	3.55	Irr
2403	07 32 05.00	65 42 42.0	17.78	10.96	Sc
4236	12 14 32.00	69 45 00.0	18.62	6.92	Irr

Obtaining a satisfactory background subtraction is the main difficulty of IR astronomy. For the observations reported here the sky brightness was typically 13.8 and 13.1 mag arcsec^{-2} at H and K' respectively, varying by several percent over the duration each source was observed. A careful monitoring of the sky is thus necessary, requiring the use of mosaicing techniques in which almost an equal amount of time is devoted to the target of interest and to the surrounding sky. Mosaic maps were obtained by programming the telescope pointing along a pattern selected ad-hoc for each galaxy according to its shape and size (see Fig. 1).
NGC 2366 (whose angular size is comparable with the MAGIC field of view) was observed alternating 8 fields centered on the target (displaced one-another by 10 arcsec) with 4 observations of the sky taken 7 arcmin to the N and S of the galaxy. Each pointing was observed for 42 s in H (40 s in K') by adding 14 (20) elementary integrations of 3 (2) s. The whole mosaic pattern was repeated twice giving a total of 672 (640) s integration on source and 336 (320) on the sky.
The galaxy NGC 2403, which has an angular extent of 18×11 arcmin^2, was mosaiced in three overlapping on-source fields taken at equal declination and displaced by $\sim 5'$ in right ascension. Each on-source field was followed by sky measurement taken at equal right ascension, displaced by 10 arcmin from the galaxy. The whole mosaic pattern was repeated twice in the K' band, but the W subframes were not combined with the central and E ones because affected by residual large-scale inhomogeneities (see Fig. 2). The total integration time was 126 s in H (240 s in K') on source (and an equal amount on the sky).
Similarly, the galaxy NGC 4236 (angular extent of 18×7 arcmin^2) was mosaiced in three overlapping on-source fields taken along the galaxy major axis, dithered by

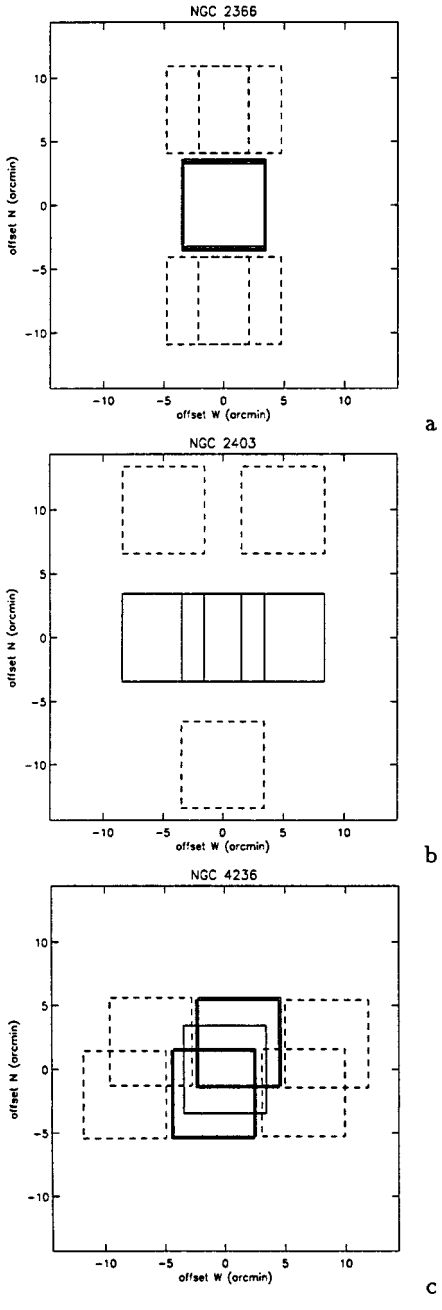

Fig. 1. Mosaic patterns for NGC 2366 **a)**, NGC 2403 **b)**, NGC 4236 **c)**

2.5 arcmin. Each on-source field was followed by sky measurement taken at equal declination, on each side of the galaxy. We integrated on the two peripheral pointings twice as long as on the central region. Since this pattern was repeated, the total integration time was 420 s in H (400 s in K') on source (and 4/5 of that on the sky).

The observations were calibrated and transformed into the H photometric system and to K' using the three standard stars HD 40335, HD 84800 and HD 106965 in the catalogue of Elias et al. (1982), observed hourly along the night.

The calibration stars were observed with a pointing sequence which consisted of five positions, starting with the star near the center of the array, followed by positioning the star in each of the four array quadrants. The telescope was defocused to avoid saturation. Only HD 40335 has a reference K' mag (Wainscoat & Cowie 1992). For HD 84800 and HD 106965, having almost null spectral slopes ($H - K = 0.00$ and 0.02 mag respectively), we assumed $K - K' = 0$.

The typical uncertainty of the photometric zero points is 0.03 mag. We also assessed the accuracy of our flat field correction by determining the differences of the star brightness at the five positions of the observing pattern. No significant differences were devised within 0.022 mag.

2.1. Image analysis

The reduction of two-dimensional IR frames follows a procedure based on the IRAF data reduction package developed by NOAO and on the SAOIMAGE and PROS packages developed at the Center for Astrophysics.

To remove the detector response each image is processed as follows. Two sets of flat-field exposures were obtained on the telescope dome with (lamp-on) and without (lamp-off) illumination with a quartz lamp. The response of the detector alone is contained in the normalized frame $\mathrm{FF} = [(\mathrm{lamp}-\mathrm{on}) - (\mathrm{lamp}-\mathrm{off})]/\langle(\mathrm{lamp}-\mathrm{on}) - (\mathrm{lamp}-\mathrm{off})\rangle$. For each galaxy all the sky exposures (SKY_i) are combined using a median filter to obtain the image $\langle\mathrm{SKY}\rangle$ if the deviation among their mean values $\langle c_{\mathrm{sky}}\rangle_i$ is smaller than 5% of their average. Otherwise, three contiguous sky measures are used. This allows removal of bad pixels and of unwanted star images. The mean counts $\langle c_{\mathrm{T}}\rangle_i$ and $\langle c_{\mathrm{sky}}\rangle$ are determined, rispectively for the i^{th} target observations and the median sky. Individual "normalized" $\langle\mathrm{SKY}\rangle_i$ frames are produced such that $\langle\mathrm{SKY}\rangle_i = \langle\mathrm{SKY}\rangle \times \langle c_{\mathrm{T}}\rangle_i / \langle c_{\mathrm{sky}}\rangle$. This allows removal of the time variations of the sky level (which are usually of the order of 5% during a full mosaic measurement), but introduces an (additive) off-set to the background which is subsequently removed.

Each target frame (T_i) is then processed to obtain a flat-field, sky subtracted, corrected frame: $T_{i,\mathrm{corr}} = [T_i - \langle\mathrm{SKY}\rangle_i]/\mathrm{FF}$. The individual $T_{i,\mathrm{corr}}$ target frames are then registered using field stars and combined together with a median filter. This allows removal of the bad pixels in the final combined image. Star-subtracted frames are produced by manual "editing" of the contribution from pointlike sources which are clearly not associated with the target galaxies, being most probably stars of our Galaxy. Extended features, possibly associated with HII regions belonging to the target galaxies are not subtracted.

Figure 2 gives a grey-scale/contour representation of the three galaxies under study, smoothed with a 0.8 pixel gaussian. For each galaxy we give the H and K' mosaics. The faintest levels shown are 21.5 (H) and 21.0 (K') mag arcsec^{-2} for NGC 2366 (Fig. 2a) and NGC 4236 (Fig. 2c) and 20.0 (H and K') mag arcsec^{-2} for NGC 2403 (Fig. 2b), with a step of 0.5 mag arcsec^{-2}. These limits are consistent with the rms of each image (see further here). The orientation of the frames is such that North is up and East to the left.

Special care was taken in determining the image properties. This analysis is summarized in Table 2. For each galaxy (and band-pass) we give the total on target integration time, followed by the estimate of the seeing, by the sky brightness and by the background noise on a scale of 4×200 pixel, i.e. not much smaller than the scale of the measured galaxies. This figure, varying from 0.03% to 0.16% of the sky, represents the dominant source of error in low S/N regions. The large-scale noise carachteristics and those determined on a much smaller angular scale (10×10 pixel) are in agreement.

Table 2. Image characteristics

NGC	band	t_{exp} s	seeing arcsec	sky mag arcsec^{-2}	rms mag arcsec^{-2}
2366	H	672	2.1	13.78	22.12
2366	K′	640	3.3	13.01	21.78
2403	H	126	2.1	13.86	20.77
2403	K′	240	2.7	13.11	20.64
4236	H	420	2.4	13.80	21.66
4236	K′	400	3.2	13.03	21.06

3. Results

3.1. Circular aperture photometry

A growth curve is first derived for each object by integrating the counts in concentric circular rings of increasing diameter, centered at the coordinates given in Table 1. The obtained H band growth curves, transformed from counts to magnitudes, are compared with the multiaperture photometry available from the literature, in order to check our photometric calibration.

Figures 3a-c give the H band growth curves of NGC 2366, NGC 2403 and NGC 4236 respectively. These measurement were obtained after subtracting all stars in the fields.

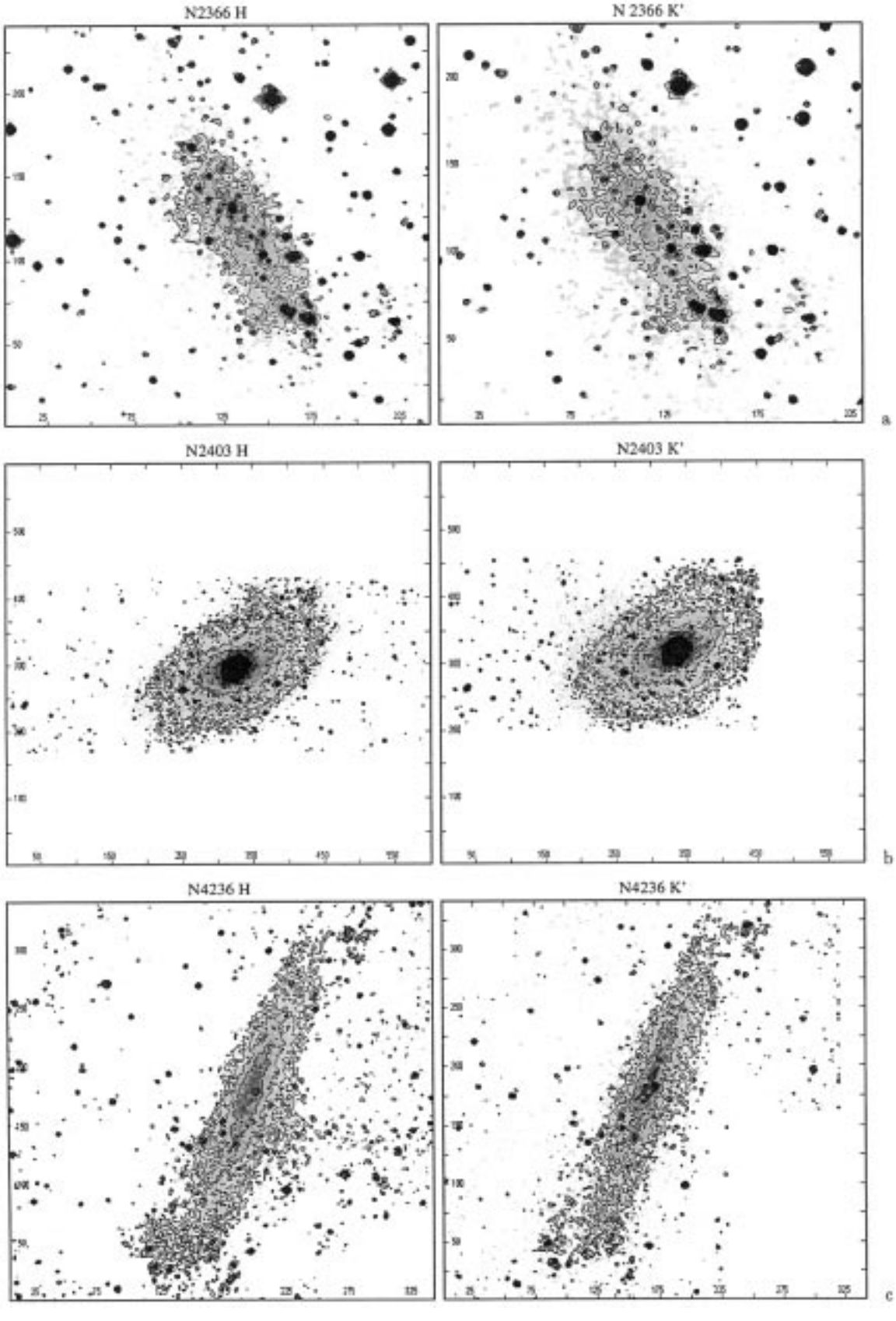

Fig. 2. Grey-scale rapresentations and contour levels of h and K' band images of NGC 2366 **a)**, NGC 2403 **b)**, NGC 4236 **c)**

The maximum diameters shown are set by the limiting surface brightness given in Table 2. The aperture photometry of AA80 is also shown in the figures (open stars).

For NGC 2366, our and the reference photometric points

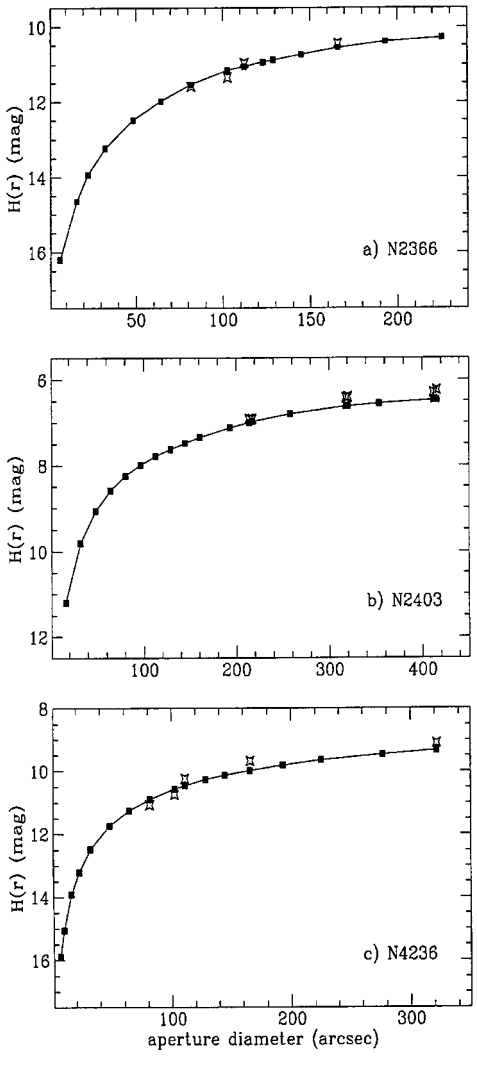

Fig. 3. H band growth curves of NGC 2366 **a)**, NGC 2403 **b)**, NGC 4236 **c)**. (Filled squares = this work; open stars = AA80 reference aperture photometry - see text)

are in satisfactory agreement.

For NGC 2403 the agreement between our measurement and the reference ones is satisfactory within an aperture of 200 arcsec. At larger diameters our growth curve is fainter than that of AA80 by 0.3 mag. AA80 photometry is obtained after removal of the 2 bright stars near the nucleus, while our is obtained with subtraction of all stars. The discrepancy reduces to ∼0.1 mag if we use similar star removal criteria.

For NGC 4236 the discrepancy with the reference photometry is ∼0.35 mag (only 0.1 mag due to star removal).

Since the K' measurements, which cannot be compared with previous photometry, were done in close sequence with the H ones, we assume that they are as well calibrated.

A comparison between the extrapolated magnitudes adopted by AA80 and the results of the present work are summarized in Table 3. At $a_{-0.5}$ adopted by AA80 (Col. 2), $H_{-0.5}$ as given by AA80 is listed in Col. 3 together with the value derived in this work (Col. 4). Column 5 lists $K'_{-0.5}$.

Table 3. Photometric parameters derived by AA80 and in this work using circular apertures

	AA80		This work			
NGC	$a_{-0.5}$ arcmin	$H_{-0.5}$ mag	$H_{-0.5}$ mag	$K'_{-0.5}$ mag	H_T mag	K'_T mag
2366	2.04	10.82	10.94	10.60	9.80 ± 0.11	9.30 ± 0.13
2403	5.13	6.45	6.65	6.47	6.27 ± 0.10	6.03 ± 0.10
4236	4.68	9.08	9.46	9.27	9.00 ± 0.12	8.69 ± 0.14

3.2. Elliptically extracted profiles

Using the star-subtracted frames, the surface brightness profiles are determined by averaging the brightness distribution in concentric elliptical annuli of fixed center, position angle and ellipticity. The position angle and ellipticity of the ellipse were determined from the H band ∼21 mag arcsec^{-2} isophotes of the galaxy under study. For NGC 2366 and NGC 2403 the latter quantity corresponds to the one determined optically. For NGC 4236 we adopt the optical ellipticity.

For several reasons we prefer this rather simple procedure to the more sophisticated ones in which the parameters of the fitted ellipses are not kept constant because: i) for spiral-Irr galaxies isodensity contours cannot be fitted with ellipses (see also de Jong & van der Kruit 1994); ii) an accurate error analysis requires keeping track of parameters such as the area of the ellipse, which is not done by the more sophisticated tools available in IRAF.

Starting from an inner ellipse of size comparable with the seeing disk, we draw a set of annuli, increasing the major axis by fixed amounts. In each ring we compute the total number of counts and the total number of pixels. The statistical uncertainties on the net counts in each annulus are computed as in Gavazzi et al. (1994).

The photometric parameters determined along elliptical rings are summarized in Table 4, as follows:

Column 1: NGC name;

Column 2: Position Angle of the galaxy major axis (measured Eastwards from North) used to derive the surface brightness profiles;

Column 3: ellipticity $(1 - b/a)$ of the rings used to derive the surface brightness profiles;

Table 4. Differential and integrated magnitudes derived along elliptical annuli

NGC	P.A. ^{o}	ϵ 1-b/a	radius arcsec	μ_H mag arcsec^{-2}	m_H mag	$\mu_{K'}$ mag arcsec^{-2}	$m_{K'}$ mag
2366	30	0.52	1.6	20.79	19.31	20.17	18.69
			4.8	20.73	16.88	20.37	16.48
			8.0	20.56	15.65	20.37	15.38
			11.3	20.43	14.82	20.22	14.58
			14.5	20.25	14.16	20.13	13.97
			17.7	20.27	13.67	20.05	13.48
			20.9	20.49	13.35	20.29	13.15
			24.1	20.45	13.05	20.27	12.86
			27.4	20.49	12.79	20.27	12.59
			30.6	20.52	12.57	20.26	12.36
			33.8	20.66	12.39	20.30	12.16
			37.0	20.67	12.22	20.39	11.98
			40.2	20.70	12.07	20.50	11.83
			43.5	20.84	11.94	20.55	11.70
			46.7	20.95	11.83	20.68	11.58
			49.9	20.99	11.72	20.70	11.47
			53.1	20.97	11.62	20.76	11.37
			56.3	21.01	11.52	20.65	11.27
			59.6	21.02	11.43	20.70	11.17
			62.8	21.03	11.34	20.75	11.08
			66.0	21.15	11.26	20.81	10.99
			69.2	21.11	11.18	20.77	10.91
			72.4	20.84	11.08	20.50	10.81
			75.7	21.13	11.01	20.75	10.73
			78.9	21.31	10.95	20.96	10.66
			82.1	21.53	10.90	21.11	10.61
			85.3	21.60	10.86	21.18	10.56
			88.5	21.47	10.81	21.12	10.50
			91.8	21.35	10.75	21.01	10.45
			95.0	21.20	10.69	20.89	10.38
			98.2	21.38	10.63	21.01	10.33
			101.4	21.85	10.60	21.15	10.28
			104.6	21.68	10.56	21.19	10.23
			107.9	21.53	10.52	21.06	10.18
			111.1	21.49	10.47	20.95	10.13
			114.3	21.83	10.44	21.23	10.08
			117.5	22.09	10.41	21.53	10.05
			120.7			21.69	10.02
2403	124	0.49	1.6	16.98	15.43	16.80	15.26
			4.8	16.93	13.00	16.80	12.86
			8.0	16.96	11.91	16.84	11.79
			11.3	17.00	11.20	16.86	11.07
			14.5	17.05	10.69	16.90	10.55
			17.7	17.08	10.28	16.95	10.14
			20.9	17.17	9.95	17.03	9.81
			24.1	17.21	9.67	17.09	9.54
			27.4	17.29	9.44	17.14	9.31
			30.6	17.36	9.24	17.22	9.10
			33.8	17.42	9.06	17.31	8.93
			37.0	17.52	8.91	17.38	8.78
			40.2	17.58	8.77	17.45	8.64
			43.5	17.66	8.65	17.53	8.52

Table 4. continued

NGC	P.A. °	ϵ 1-b/a	radius arcsec	μ_H mag arcsec^{-2}	m_H mag	$\mu_{K'}$ mag arcsec^{-2}	$m_{K'}$ mag
			46.7	17.73	8.54	17.58	8.40
			49.9	17.77	8.43	17.66	8.30
			53.1	17.85	8.34	17.70	8.20
			56.3	17.88	8.25	17.77	8.12
			59.6	17.94	8.17	17.81	8.03
			62.8	18.00	8.09	17.86	7.96
			66.0	18.08	8.02	17.90	7.88
			69.2	18.10	7.95	17.98	7.82
			72.4	18.19	7.89	18.03	7.75
			75.7	18.24	7.83	18.08	7.69
			78.9	18.26	7.77	18.10	7.63
			82.1	18.32	7.72	18.16	7.58
			85.3	18.35	7.67	18.19	7.53
			88.5	18.38	7.62	18.23	7.48
			91.8	18.45	7.57	18.26	7.43
			95.0	18.48	7.53	18.31	7.38
			98.2	18.48	7.48	18.35	7.34
			101.4	18.55	7.44	18.36	7.30
			104.6	18.61	7.40	18.41	7.26
			107.9	18.62	7.37	18.43	7.22
			111.1	18.68	7.33	18.49	7.18
			114.3	18.67	7.29	18.49	7.14
			117.5	18.72	7.26	18.55	7.11
			120.7	18.77	7.23	18.59	7.07
			124.0	18.82	7.20	18.63	7.04
			127.2	18.84	7.17	18.66	7.01
			130.4	18.87	7.14	18.69	6.98
			133.6	18.91	7.11	18.71	6.95
			136.8	18.92	7.08	18.77	6.92
			140.1	19.00	7.05	18.82	6.90
			143.3	19.04	7.03	18.85	6.87
			146.5	19.10	7.00	18.92	6.85
			149.7	19.13	6.98	18.95	6.82
			152.9	19.17	6.96	19.00	6.80
			156.2	19.18	6.94	19.00	6.78
			159.4	19.23	6.92	19.02	6.76
			162.6	19.26	6.89	19.07	6.73
			165.8	19.26	6.87	19.12	6.71
			169.0	19.31	6.85	19.14	6.69
			172.3	19.33	6.84	19.14	6.67
			175.5	19.34	6.82	19.16	6.65
			178.7	19.40	6.80	19.15	6.63
			181.9	19.40	6.78	19.20	6.62
			185.1	19.42	6.76	19.18	6.60
			188.4	19.48	6.74	19.27	6.58
			191.6	19.53	6.73	19.32	6.56
			194.8	19.56	6.71	19.34	6.55
			198.0	19.63	6.70	19.42	6.53
			201.2	19.67	6.68	19.46	6.52
			204.5	19.68	6.67	19.47	6.50
			207.7	19.73	6.66	19.51	6.49
			210.9	19.74	6.64	19.51	6.47

Table 4. continued

NGC	P.A. ^{o}	ϵ 1-b/a	radius arcsec	μ_H mag arcsec^{-2}	m_H mag	$\mu_{K'}$ mag arcsec^{-2}	$m_{K'}$ mag
4236	154	0.63	1.6	19.53	18.34	19.32	18.12
			4.8	19.69	16.09	19.50	15.89
			8.0	19.73	15.02	19.46	14.77
			11.3	19.69	14.28	19.46	14.04
			14.5	19.67	13.72	19.54	13.53
			17.7	19.67	13.28	19.52	13.10
			20.9	19.70	12.92	19.53	12.74
			24.1	19.71	12.62	19.55	12.44
			27.4	19.78	12.36	19.65	12.20
			30.6	19.82	12.14	19.68	11.98
			33.8	19.81	11.94	19.69	11.78
			37.0	19.90	11.76	19.73	11.61
			40.2	19.92	11.60	19.81	11.46
			43.5	20.00	11.46	19.84	11.31
			46.7	20.05	11.34	19.94	11.19
			49.9	20.09	11.22	20.01	11.08
			53.1	20.16	11.11	20.04	10.98
			56.3	20.21	11.02	20.04	10.88
			59.6	20.23	10.92	20.08	10.78
			62.8	20.29	10.84	20.12	10.70
			66.0	20.30	10.75	20.17	10.61
			69.2	20.36	10.68	20.20	10.54
			72.4	20.45	10.61	20.24	10.46
			75.7	20.48	10.54	20.30	10.40
			78.9	20.49	10.48	20.32	10.33
			82.1	20.47	10.41	20.28	10.26
			85.3	20.58	10.36	20.38	10.20
			88.5	20.61	10.30	20.39	10.15
			91.8	20.63	10.25	20.50	10.09
			95.0	20.68	10.20	20.53	10.04
			98.2	20.76	10.15	20.57	10.00
			101.4	20.79	10.11	20.64	9.95
			104.6	20.91	10.07	20.65	9.91
			107.9	20.90	10.03	20.76	9.87
			111.1	20.93	9.99	20.74	9.83
			114.3	21.01	9.96	20.79	9.79
			117.5	20.98	9.92	20.74	9.76
			120.7	21.01	9.89	20.87	9.72
			124.0	21.06	9.85	20.82	9.69
			127.2	21.13	9.82	20.89	9.65
			130.4	21.15	9.79	20.99	9.62
			133.6	21.30	9.76	21.06	9.59
			136.8	21.37	9.74	21.02	9.57
			140.1	21.38	9.72	21.05	9.54
			143.3	21.42	9.69		
			146.5	21.46	9.67		
			149.7	21.38	9.64		
			152.9	21.48	9.62		
			156.2	21.42	9.60		
			159.4	21.46	9.58		

Column 4: projected distance in arcsec along the major axis, truncated at the radius corresponding to a surface brightness equivalent to 1 σ of the sky;
Columns 5-6: H band surface brightness and integrated magnitude;
Columns 7-8: K' band surface brightness and integrated magnitude.
These magnitudes are measured quantities and are not corrected to the face-on value.

Figure 4 gives the differential H and K' profiles in mag arcsec^{-2}, obtained by azimuthal integration along elliptical annuli and the differential $H-K'$ color profile. The horizontal scale of panels B and C gives the projected distance in arcsec as measured from the galaxy center along the major axis of the ellipse. The profiles are truncated at the limiting surface brightness of Table 2. The wiggles bteween 70 and 120 arcsec in the profiles of NGC 2366 are due to HII regions. The $H-K'$ color index for the three galaxies is in agreement with $< H-K' >= 0.26 \pm 0.11$ mag found by Boselli et al. (1997) for Virgo galaxies.

Columns 6 and 7 of Table 3 list the H and K' band asymptotic magnitudes, with their uncertainties (including the zero point and the error introduced by the extrapolation to infinity). An exponential disk was fit to the radial surface brightness profile in the intermediate radial range, where the profile shows an exponential shape. The total magnitude was computed by integrating the counts along elliptical annuli up to the last useful radius (see Cols. 5 and 7 of Table 4) and by adding the the contribution derived from the exponential fit from this radius to infinity.

Acknowledgements. We thank the MAGIC team at MPI für Astronomie for their skilful operational support and for several helpful discussions about data reduction. A.B. is supported by a stipendium from the Deutsche Argentur für Raumfartengelegenheiten (DARA), GmbH, Bonn, Germany, (grant # 50-OR-95018).

References

Aaronson M., Mould J., Huchra J., 1980, ApJ 237, 655 (AA80)
Aaronson M., Bothun G., Mould J., et al., 1986, ApJ 302, 536
Boselli A., Tuffs R., Gavazzi G., Hippelein H., Pierini D., 1997, A&AS 121, 507
de Jong R., van der Kruit P., 1994, A&AS 106, 451
de Vaucouleurs G., de Vaucouleurs A., Corwin H., 1976, Second Reference Catalogue of Bright Galaxies. The University of Texas, Austin (RC2)
Elias J.H., Frogel J.A., Matthews K., Neugebauer G., 1982, AJ 87, 1029
Freedman W., 1990, ApJ 355, L35
Gavazzi G., Scodeggio M., Boselli A., Trinchieri G., 1991, ApJ 382, 19
Gavazzi G., Garilli B., Carrasco L., Boselli A., Cruz Gonzalez I., 1994, A&AS 104, 271
Herbst T., Beckwith S., Birk C., et al. 1993, SPIE 1946
Peletier R., Willner S., 1993, ApJ 418, 626
Tully B., Fisher J., 1977, A&A 54, 661
Wainscoat R., Cowie L., 1992, AJ 103, 332

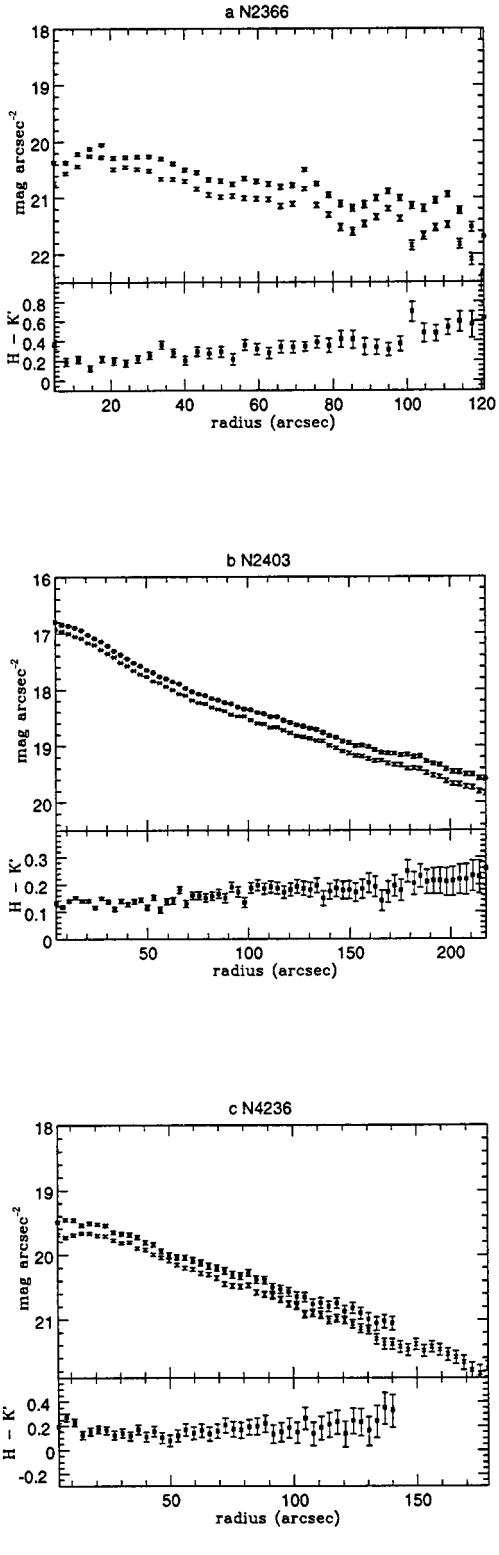

Fig. 4. Light profiles of NGC 2366 **a)**, NGC 2403 **b)**, NGC 4236 **c)**. (Filled squares = K' data; crosses = H data)